

## Highly Coherent Electron Beam from a Laser-Triggered Tungsten Needle Tip

Dominik Ehberger,<sup>1,2,\*</sup> Jakob Hammer,<sup>1,2</sup> Max Eisele,<sup>2,†</sup> Michael Krüger,<sup>1,2,‡</sup>

Jonathan Noe,<sup>3</sup> Alexander Högele,<sup>3</sup> and Peter Hommelhoff<sup>1,2,4,§</sup>

<sup>1</sup>*Department of Physics, Friedrich Alexander University Erlangen-Nuremberg, Staudtstrasse 1, D-91058 Erlangen, Germany, EU*

<sup>2</sup>*Max Planck Institute of Quantum Optics, Hans-Kopfermann-Strasse 1, D-85748 Garching/Munich, Germany, EU*

<sup>3</sup>*Fakultät für Physik and Center for NanoScience (CeNS), Ludwig-Maximilians-Universität München, Geschwister-Scholl-Platz 1, 80539 München, Germany, EU*

<sup>4</sup>*Max Planck Institute for the Science of Light, Günther-Scharowsky-Strasse 1/ Building 24, D-91058 Erlangen, Germany, EU*

(Received 10 December 2014; published 5 June 2015)

We report on a quantitative measurement of the spatial coherence of electrons emitted from a sharp metal needle tip. We investigate the coherence in photoemission triggered by a near-ultraviolet laser with a photon energy of 3.1 eV and compare it to dc-field emission. A carbon nanotube is brought into close proximity to the emitter tip to act as an electrostatic biprism. From the resulting electron matter wave interference fringes, we deduce an upper limit of the effective source radius both in laser-triggered and dc-field emission mode, which quantifies the spatial coherence of the emitted electron beam. We obtain  $(0.80 \pm 0.05)$  nm in laser-triggered and  $(0.55 \pm 0.02)$  nm in dc-field emission mode, revealing that the outstanding coherence properties of electron beams from needle tip field emitters are largely maintained in laser-induced emission. In addition, the relative coherence width of 0.36 of the photoemitted electron beam is the largest observed so far. The preservation of electronic coherence during emission as well as ramifications for time-resolved electron imaging techniques are discussed.

DOI: [10.1103/PhysRevLett.114.227601](https://doi.org/10.1103/PhysRevLett.114.227601)

PACS numbers: 79.60.Jv, 07.77.Ka, 42.25.Kb

Coherent electron sources are central to studying microscopic objects with highest spatial resolution. They provide electron beams with flat wave fronts that can be focused to the fundamental physical limit given by matter wave diffraction [1]. Currently, time-resolved electron-based imaging is being pursued with great effort, both in real-space microscopy [2,3] and in diffraction [4,5]. However, the spatial resolution in time-resolved electron microscopy is about 2 orders of magnitude lower than its dc counterpart [6], which reaches below 0.1 Å [7]. Combining highest spatial resolution with time resolution in the picosecond to (sub)femtosecond range requires spatially coherent electron sources driven by ultrashort laser pulses. Although laser-driven metal nanotips promise to provide coherent electron pulses with highest time resolution, a quantitative study of their spatial coherence has been elusive. Here we demonstrate that photoemitted electrons from a tungsten nanotip are highly coherent.

Thus far, no time-resolved electron-based imaging instrument fully utilizes the coherence capabilities provided by nanotip electron sources. Meanwhile, nanotips operated in dc-field emission have been known and employed in practical applications for almost half a century for their paramount spatial coherence properties [8]. Thence, highest resolution microscopy as well as coherent imaging, such as holography and interferometry, have long been demonstrated in dc-field emission [1,9,10]. Here we investigate

whether these concepts can be inherited to laser-driven nanotip sources by comparing the spatial coherence of photoemitted electron beams to their dc counterparts. This would enable time-resolved high-resolution imaging, but may also herald fundamental studies based on the generation of quantum degenerate electron beams [11].

The spatial coherence of electron sources is commonly quantified by means of their effective source radius  $r_{\text{eff}}$ . It equals the radius of a virtual incoherent emitter that resembles the coherence properties of the real emitter. As discussed below,  $r_{\text{eff}}$  is inversely proportional to the transverse coherence length  $\xi_{\perp}$  of the electron beam. A virtual source is formed in a finite area where electron trajectories intersect when extrapolating their paths back into the metal tip [Fig. 1(d)]. For tungsten field emitters, typical values for  $r_{\text{eff}}$  are on the order of 1 nm and the smallest reported is down to 0.4 nm, significantly smaller than the geometrical tip radius that is typically in the range of a few tens of nanometers [1,12].

dc-field and laser-driven emission occur due to fundamentally different emission processes [Fig. 1(a)] [13]. The former is a tunneling process through a static potential barrier, covered within the Fowler-Nordheim framework [14], whereas a variety of laser-driven emission processes exist. They are distinguishable into linear one-photon emission and nonlinear multiphoton and tunneling processes, with the respective prominent examples of Einstein's

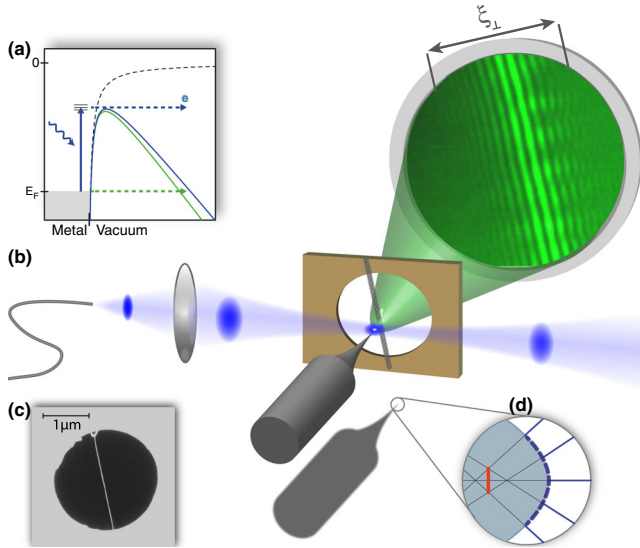


FIG. 1 (color online). Schematic of the experimental setup. (a) Illustration of one-photon photoemission (blue) and dc-field emission (green). Electrons from states around the Fermi level  $E_F$  are excited by laser irradiation and emitted over the barrier, which is lowered due to the Schottky effect. At sufficiently high dc fields the barrier becomes narrow enough to permit direct tunneling through it, giving rise to dc-field emission. (b) Ultrahigh vacuum setup. A near-UV laser beam (photon energy of 3.1 eV) coupled into the chamber via a polarization maintaining fiber is focused onto the apex of a tungsten tip. Interference patterns are obtained on the microchannel plate detector after the electrons have passed a freestanding carbon nanotube (CNT) beam splitter placed in close vicinity to the tip. (c) Scanning electron microscope image of a CNT grown over a hole of a SiN membrane. (d) Sketch illustrating the formation of a virtual (or effective) source behind the tip's apex as indicated by five exemplary electron trajectories (solid black lines). The diameter of the virtual source (vertical red full line) is substantially smaller than the geometrical source size (blue dashed line).

photoelectric effect and multiphoton emission [15]. The effective source radius is highly sensitive to the shape of the electron trajectories in close vicinity of the tip apex [16], and hence to the emission process. As a result, the coherence properties in photoemission might be drastically different from dc-field emission.

To compare the coherence properties of a monocrystalline tungsten tip electron emitter with a radius of  $\sim 10$  nm in laser-triggered and dc-field emission, we record electron matter wave interference images in both emission modes. We use a freestanding carbon nanotube (CNT) as an electron beam splitter, which acts as a biprism filament with nanometer radius [10]. It splits the wave front of the electron matter wave in two parts, which are then overlapped at the electron detector, giving rise to interference fringes on the detector screen [12]. A scanning electron microscope image of a single, freestanding CNT on a holey silicon nitride membrane is shown in Fig. 1(c) (see Supplemental Material [17] for details). The electrically

grounded CNT is brought into the electron beam path at a typical distance of less than one micrometer from the tip, resembling a point projection microscopy configuration, that is also commonly used for electron holography [21,22]. The CNT and the gold-coated holey silicon nitride membrane act as a counter electrode for the biased tip. Electron interference can be observed in conventional dc-field emission as well as in the laser-triggered mode when a near-UV laser beam is focused on the tip's apex [see Fig. 1(b) and Supplemental Material [17] for a detailed discussion of the pertinent imaging regimes].

An upper bound for  $r_{\text{eff}}$  is obtained by measuring the full width  $\xi_{\perp}$  of coherent illumination at the detector screen. It can be deduced by identifying the distance between the outermost interference fringes, observed perpendicular to the orientation of the CNT [23]. The van Cittert–Zernicke theorem relates  $\xi_{\perp}$  and the effective source radius  $r_{\text{eff}}$  for an incoherent emitter with Gaussian intensity profile [23,24]:

$$r_{\text{eff}} = \frac{\lambda_{\text{dB}} \cdot l_{s-d}}{\pi \cdot \xi_{\perp}}. \quad (1)$$

Here,  $\lambda_{\text{dB}}$  is the electron de Broglie wavelength and  $l_{s-d}$  the source-detector distance.

Ideally, an electron source should exhibit a narrow (longitudinal) momentum distribution to reduce chromatic effects in subsequent electron optics. Hence, in order to achieve efficient electron emission with little excess momentum, we match the Schottky-lowered barrier at the metal-vacuum interface, which is tunable by means of the tip voltage, to the photon energy ( $E_{\text{ph}} = 3.1$  eV) of the focused laser light. Here the barrier height is set to  $2.8 \pm 0.1$  eV, closely above the onset of dc-field emission and yielding the highest photoemission probability with negligible dc component. The experiments are performed with a pulsed laser (second harmonic of 130 fs long pulses derived from a 2.7 MHz repetition rate long-cavity Ti:sapphire oscillator) and a high-power cw-diode laser source (400 mW at 405 nm) to boost the electron current for the effective source radius measurements.

Electron interference patterns in laser-triggered and dc-field emission are shown in Figs. 2(a) and 2(b), respectively, recorded at the identical CNT position with a tip-sample distance of less than  $1 \mu\text{m}$ . Clearly, interference fringes that are aligned parallel to the CNT are observed in both modes. A tip voltage of  $U_{\text{tip}} = -41$  V is chosen in laser-induced emission, such that the barrier is lowered for efficient photoemission. For dc-field emission a voltage of  $U_{\text{tip}} = -53$  V is applied, leading to a comparable field emission electron current as in photoemission.

The panels in Figs. 2(c) and 2(d) show line profiles obtained from integrating the count rate parallel to the fringes in the marked area. The spatial coherence width is obtained from these line profiles. For photoemission we obtain  $\xi_{\perp}^{\text{ph}} \geq 5.9$  mm at a CNT-screen distance of 79.5 mm.

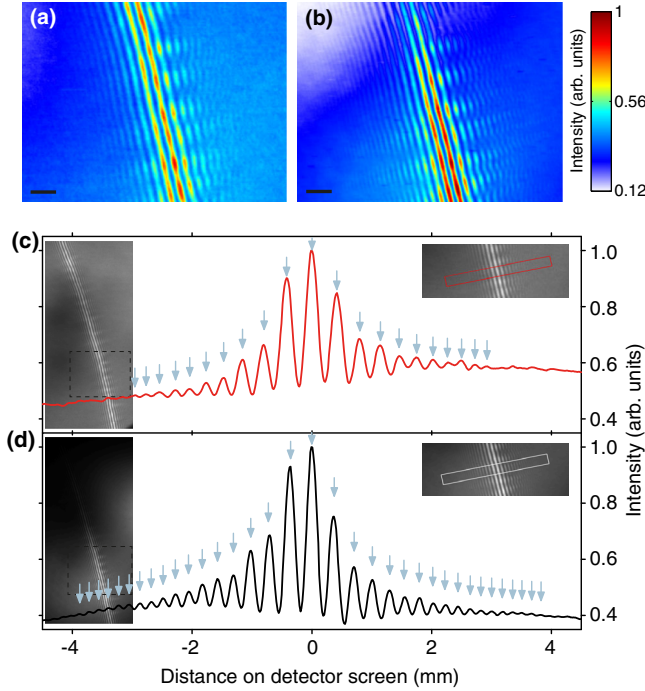


FIG. 2 (color online). Electron interference fringes on the detector screen. (a) Laser-triggered electron emission at a bias voltage of  $U_{\text{tip}} = -41$  V. Without laser illumination no electrons are observed at this voltage. Scale bar is 1 mm on the detector screen. (b) dc-field emission ( $U_{\text{tip}} = -53$  V). Images are obtained by superimposing 200 individual images that have been corrected for slow linear drifts (see Supplemental Material [17]). A modulation of the fringe pattern along the CNT direction is also clearly discernible, arising from local distortions of the CNT and locally enhanced dc fields. Line profiles of the interference fringes are integrated perpendicular to the orientation of the CNT with laser-triggered (c) and dc-field emission source (d). The box in the right-hand inset indicates the  $9.3 \text{ mm}^2$  large integration area. The left-hand inset shows a larger detector image. At least 21 fringes in the laser-triggered mode and 35 in dc-field emission mode are visible as indicated with arrows. The slightly finer spacing in dc-field emission is due to the smaller electron de Broglie wavelength (see Supplemental Material [17]).

With  $\lambda_{\text{dB}} = 1.8 \text{ \AA}$ , the effective source radius equals  $r_{\text{eff}}^{\text{ph}} \leq 0.80 \pm 0.05 \text{ nm}$ .

In the dc-field emission mode a very comparable value of the coherence width is deduced with  $\xi_{\perp} \geq 7.7 \text{ nm}$ , albeit slightly larger [Fig. 2(d)]. With  $\lambda_{\text{dB}} = 1.7 \text{ \AA}$ , the effective source radius equals  $r_{\text{eff}}^{\text{dc}} \leq 0.55 \pm 0.02 \text{ nm}$ , in line with previously published values [12,23].

Clearly, the source radii in laser-triggered and dc-field emission mode differ only slightly, even though the emission process is qualitatively different. Furthermore, in both cases the effective source radius is about an order of magnitude smaller than the geometrical source radius. For comparison, the record resolution laser-triggered electron microscope employs a fully illuminated flat  $\text{LaB}_6$  cathode of a few tens of microns in diameter [25,26]. In this

configuration the effective source radius equals the geometrical source radius, given by the smaller of either the laser spot size or the dimensions of the cathode.

The relative coherence width  $K$ , namely the ratio of  $\xi_{\perp}$  to the electron beam radius  $R_I$ , is a conserved quantity in electron optics [24]. Thus, it allows us to calculate  $\xi_{\perp}$  for any given beam size, in particular, for arbitrary focusing conditions at a sample. With  $R_I = 16 \text{ nm}$  ( $1/e^2$  radius of the electron beam) at the detector, the relative coherence width of the photoemitted beam equals 0.36, representing the highest value reported for  $K$  of a laser-triggered electron source to date. It benefits largely from the use of a monocrystalline tip, which exhibits a low rms divergence of the emitted beam of  $\sim 6^\circ$  in photoemission and  $\sim 3^\circ$  in dc-field emission. In the latter case electrons are predominantly emitted from the tungsten [310] crystallographic plane, which has the lowest work function. With  $E_{\text{ph}} = 3.1 \text{ eV}$  and dc fields closely below the field emission threshold, electrons from crystal planes with work functions up to 4.8 eV are photoemitted over the Schottky-lowered barrier [Fig. 1(a)]. In the experiment this manifests itself by the higher divergence of the photoemitted electron beam. Consequently, the geometrical rms emittance of the photoemitted beam of  $0.08 \text{ nm rad}$  (at 44 eV) is larger than in dc-field emission ( $0.03 \text{ nm rad}$  at 53 eV). However, it should be possible to reduce the emittance in photoemission by further decreasing the tip bias and hence the static field at the apex leading to predominant emission from the [310] crystallographic plane like in dc-field emission, provided that the decrease in emission efficiency that goes along with an increased barrier height can be tolerated.

With increasing electron current it can be expected that the effective source size increases due to space charge and stochastic Coulomb electron-electron repulsion [16]. Strictly, these effects come into play for more than one electron per pulse emitted from the tip. Hence, most conservatively, the maximum current attainable with the highest spatial coherence is set by the repetition rate  $f_{\text{rep}}$  of the laser. For instance, laser pulses with  $f_{\text{rep}} = 100 \text{ MHz}$  inducing emission of one electron per pulse yield a time-averaged current of 16 pA. Even though this value is low compared to the electron current emitted from standard field emission guns, electron imaging with a stably aligned laser beam, as demonstrated here, remains highly possible as demonstrated in time-resolved scanning electron microscopy [27]. The restriction to one electron per pulse, however, also prevents other unwanted detrimental effects such as temporal electron pulse broadening due to Coulomb repulsion [28]. In this experiment, the required minimum peak fluence  $2E_P/(\pi w_0^2)$  to obtain one electron per pulse without dc contributions equals  $0.2 \text{ J/cm}^2$ , with the pulse energy  $E_P$  and the  $1/e^2$  beam waist radius  $w_0$ . Note that many more than one electron per pulse can be drawn from the tip for most settings without detrimental effects on the beam quality, especially after propagation to a

sample. This, however, depends on various parameters such as tip radius, laser pulse duration, acceleration field, and electron beam path.

Next to the transverse coherence, quantified by  $r_{\text{eff}}$ , the energy spread of the electron beam  $\Delta E$  is crucially important for most applications. Here  $\Delta E$  of the photoemitted beam equals  $0.51 \pm 0.06$  eV (FWHM), less than twice as much as in dc-field emission [1]. This implies that the longitudinal coherence length is smaller by a factor of about 2 in photoemission [9], likely causing the reduced visibility of the interference pattern in Fig. 2(c) (see Supplemental Material [17]). We find that, in principle, the energy spread can be made as low as in dc-field emission with constant electron current by decreasing the dc field at the tip and simultaneously increasing the laser power (see Supplemental Material [17]). For instance, here  $\Delta E \approx 0.4$  eV is feasible with an increased barrier height of  $\sim 3.0$  eV and tripled laser fluence. We note that a decreased electron energy spread at the source is also favorable in order to prevent dispersive electron pulse broadening in vacuum. This tunability of the energy spread at the cathode is a unique feature of nanometric tip sources and, in practice, is much simpler than tuning the laser wavelength [29].

We conclude that the coherence of the electron beam in one-photon photoemission close to the threshold is almost as good as that of a dc-field emitted beam. It has been previously shown that the initial electronic states inside the metal from which the electrons originate affect the coherence of the emitted electron beam [12]. Our measurements demonstrate that the coherence of the original electronic states inside the metal is maintained in photoemission. One may thus expect that a cooled tip also provides a fully coherent beam under laser irradiation, as demonstrated in dc-field emission [12].

By virtue of the excellent coherence properties of a dc-field emitted electron beam, it was shown that the combination of point projection holography and coherent electron diffraction allows for 2 Å resolution in imaging of graphene [22]. Very recently, the first time-resolved results have been obtained in femtosecond point projection microscopy [30], ultrafast low-energy electron diffraction [31], and combinations of both [32] based on femtosecond laser-triggered tungsten field emission tips as electron sources [33–35]. In this context our findings clearly show that electron imaging devices equipped with field emission guns can be laser triggered to obtain highest temporal resolution without losing their supreme coherence and imaging properties. The excellent source properties will also be of great interest for novel laser-based electron acceleration schemes as recently demonstrated [36,37].

The authors thank H. Kaupp for discussions on electron beam coherence measurements prior to the experiment, S. Stapfner, L. Ost, and E. Weig for discussions on CNT fabrication, and J. P. Kotthaus for clean room access. This research is funded in part by the Gordon and Betty Moore

Foundation, the DFG Cluster of Excellence Munich Centre for Advanced Photonics, and the ERC Grants NearFieldAtto and QuantumCANDI.

D. E. and J. H. contributed equally to this work.

- 
- \*Now at: Ludwig-Maximilians-Universität München, Am Coulombwall 1, 85748 Garching, Germany, EU.  
dominik.ehberger@physik.uni-muenchen.de
- †Now at: Department of Physics, University of Regensburg, 93040 Regensburg, Germany, EU.
- ‡Now at: Department of Physics of Complex Systems, Weizmann Institute of Science, Rehovot 76100, Israel.
- §peter.hommelhoff@fau.de
- [1] J. Spence, *High-Resolution Electron Microscopy* (Oxford University Press, New York, 2013).
  - [2] A. H. Zewail and J. M. Thomas, *4D Electron Microscopy Imaging in Space and Time* (Imperial College Press, London, 2010).
  - [3] W. E. King, G. H. Campbell, A. Frank, B. Reed, J. F. Schmerge, B. J. Siwick, B. C. Stuart, and P. M. Weber, *J. Appl. Phys.* **97**, 111101 (2005).
  - [4] G. Sciaini and R. J. D. Miller, *Rep. Prog. Phys.* **74**, 096101 (2011).
  - [5] P. Baum, D.-S. Yang, and A. H. Zewail, *Science* **318**, 788 (2007).
  - [6] A. Yurtsever, R. M. van der Veen, and A. H. Zewail, *Science* **335**, 59 (2012).
  - [7] R. Erni, M. D. Rossell, C. Kisielowski, and U. Dahmen, *Phys. Rev. Lett.* **102**, 096101 (2009).
  - [8] A. V. Crewe, D. N. Eggenberger, J. Wall, and L. M. Welter, *Rev. Sci. Instrum.* **39**, 576 (1968).
  - [9] H. Lichte and M. Lehmann, *Rep. Prog. Phys.* **71**, 016102 (2008).
  - [10] F. Hasselbach, *Rep. Prog. Phys.* **73**, 016101 (2010).
  - [11] P. Lougovski and H. Batelaan, *Phys. Rev. A* **84**, 023417 (2011).
  - [12] B. Cho, T. Ichimura, R. Shimizu, and C. Oshima, *Phys. Rev. Lett.* **92**, 246103 (2004).
  - [13] K. L. Jensen, P. G. O’Shea, D. W. Feldman, and J. L. Shaw, *J. Appl. Phys.* **107**, 014903 (2010).
  - [14] R. H. Fowler and L. Nordheim, *Proc. R. Soc. A* **119**, 173 (1928).
  - [15] N. B. Delone and V. P. Krainov, *Multiphoton Processes in Atoms* (Springer, Berlin, 1994).
  - [16] B. Cook, T. Verduin, C. W. Hagen, and P. Kruit, *J. Vac. Sci. Technol. B*, **28**, C6C74 (2010).
  - [17] See Supplemental Material at <http://link.aps.org/supplemental/10.1103/PhysRevLett.114.227601>, which includes Refs. [18–20], for details on the experimental setup and evaluation methods.
  - [18] M. S. Hofmann, J. T. Glückert, J. Noé, C. Bourjau, R. Dehmelt, and A. Högele, *Nat. Nanotechnol.* **8**, 502 (2013).
  - [19] I.-S. Hwang, C.-C. Chang, C.-H. Lu, S.-C. Liu, Y.-C. Chang, T.-K. Lee, H.-T. Jeng, H.-S. Kuo, C.-Y. Lin, C.-S. Chang, and T. T. Tsong, *New J. Phys.* **15**, 043015 (2013).
  - [20] G. Möllenstedt and H. Düker, *Z. Phys.* **145**, 377 (1956).
  - [21] A. Beyer and A. Götzhäuser, *J. Phys. Condens. Matter* **22**, 343001 (2010).

- [22] J.-N. Longchamp, T. Latychevskaia, C. Escher, and H. W. Fink, *Phys. Rev. Lett.* **110**, 255501 (2013).
- [23] J. C. H. Spence, W. Qian, and M. P. Silverman, *J. Vac. Sci. Technol.* **12**, 542 (1994).
- [24] G. Pozzi, *Optik (Stuttgart)* **77**, 69 (1987).
- [25] B. Barwick, H. S. Park, O.-H. Kwon, J. S. Baskin, and A. H. Zewail, *Science* **322**, 1227 (2008).
- [26] Despite the state of development, a femtosecond laser-triggered electron microscope is commercially available from a large electron microscope manufacturer, indicating the expected market volume. See [www.fei.com/tecna-femto/](http://www.fei.com/tecna-femto/).
- [27] D.-S. Yang, O. F. Mohammed, and A. H. Zewail, *Proc. Natl. Acad. Sci. U.S.A.* **107**, 14993 (2010).
- [28] F. O. Kirchner, A. Gliserin, F. Krausz, and P. Baum, *Nat. Photonics* **8**, 52 (2014).
- [29] L. Kasmi, D. Kreier, M. Bradler, E. Riedle, and P. Baum, *New J. Phys.* **17**, 033008 (2015).
- [30] E. Quinonez, J. Handali, and B. Barwick, *Rev. Sci. Instrum.* **84**, 103710 (2013).
- [31] M. Gulde, S. Schweda, G. Storeck, M. Maiti, H. K. Yu, A. M. Wodtke, S. Schäfer, and C. Ropers, *Science* **345**, 200 (2014).
- [32] M. Müller, A. Paarmann, and R. Ernstorfer, *Nat. Comm.* **5**, 5292 (2014).
- [33] P. Hommelhoff, Y. Sortais, A. Aghajani-Talesh, and M. A. Kasevich, *Phys. Rev. Lett.* **96**, 077401 (2006).
- [34] P. Hommelhoff, C. Kealhofer, and M. A. Kasevich, *Phys. Rev. Lett.* **97**, 247402 (2006).
- [35] C. Ropers, D. R. Solli, C. P. Schulz, C. Lienau, and T. Elsaesser, *Phys. Rev. Lett.* **98**, 043907 (2007).
- [36] E. A. Peralta, K. Soong, R. J. England, E. R. Colby, Z. Wu, B. Montazeri, C. McGuinness, J. McNeur, K. J. Leedle, D. Walz, E. B. Sozer, B. Cowan, B. Schwartz, G. Travish, and R. L. Byer, *Nature (London)* **503**, 91 (2013).
- [37] J. Breuer and P. Hommelhoff, *Phys. Rev. Lett.* **111**, 134803 (2013).